Journal of Solid State Chemistry 263 (2018) 24–29

Contents lists available at ScienceDirect

Journal of Solid State Chemistry

journal homepage: www.elsevier.com/locate/jssc

Y_2S_3 – Y_2O_3 phase diagram and the enthalpies of phase transitions

P.O. Andreev[a,*], L.A. Pimneva[b]

[a] University of Tyumen, 6 Volodarskogo St, 625003 Tyumen, Russia
[b] Federal State budget institution of higher education "Tyumen Industrial University", 38 Volodarskogo St, 625000 Tyumen, Russia

ARTICLE INFO

Keywords:
Yttrium sulfide
Yttrium oxysulfide
Phase diagram
Thermal analysis
Melting enthalpy
Phase transformation

ABSTRACT

A phase diagram of the Y_2S_3-Y_2O_3, system has been defined from 1000 K to melts for the first time; the enthalpies of phase transitions in the systems have been determined. The monoclinic phase δ-Y_2S_3 ($P2_1/m$, a = 1.7523(8) nm, b = 0.4010(9) nm, c = 1.0170(7) nm, β = 98.60(6)°; microhardness H = 411 ± 7 HV) transforms at 1716 ± 7 K to the unquenchable high-temperature phase ξ-Y_2S_3, ΔH = 29 ± 6 J/g (7.9 KJ/mol) as determined by DSC. The quenching can't latch the Y_2S_3-phase. The melting point of Y_2S_3 is 1888 ± 7 K; ΔH = 150 ± 28 J/g (41.1 KJ/mol). Y_2OS_2 has a monoclinic structure ($P21/c$, a = 0.8256(8) nm, b = 0.6879(8) nm, c = 0.6848(8) nm, β = 99.52(6), H = 491 ± 13 HV) and melts incongruently at 1790 ± 8 K, ΔH = 190 ± 45 J/g (52 KJ/mol) by the scheme $Y_2OS_2 \leftrightarrow Y_2O_2S + L$ (16 mol% Y_2O_3). Y_2O_2S has a hexagonal structure (a = 0.3784(5) nm, c= 0.6584(4) nm, H = 654 ± 7 HV). Its congruent melting temperature is 2350 ± 40 K as determined by visual polythermal analysis (VPTA). The eutectic formed by Y_2S_3 and Y_2OS_2 phases has the composition 14.0 ± 0.5 mol% Y_2O_3 ($0.58Y_2S_3 + 0.42Y_2OS_2$) and melting temperature 1770 ± 6 K; ΔH = 215 ± 39 J/g. Between Y_2O_2S and Y_2O_3 phases, there is a eutectic with the coordinates 80 ± 1 mol% Y_2O_3 ($0.6Y_2O_2S + 0.4Y_2O_3$) and melting temperature 2150 ± 35 K (VPTA).

1. Introduction

Yttrium dioxosulfide Y_2O_2S ($1Y_2S_3$ $2Y_2O_3$), a member of Ln_2O_2S (Ln = La-Lu) family, is used as a matrix in crystal phosphor design [1,2]. The doped Y_2O_2S nanoparticles were prepared from electrospun poly(vinylpyrrolidone) composite using sulfur powder [3–5]. The morphology of Y_2O_3: Eu^{3+}; Y_2O_3: Yb^{3+}; Er^{3+} precursor particles was preserved during the synthesis. Yang et al. fabricated Y_2O_3S:Eu^{3+} nanobelts 6.7 × 125 nm^2 in size and the phosphor possessed red emission peaks at 628 and 618 nm under excitation by 325-nm UV light [3]. Han et al. manufactured hollow Y_2O_3:Eu^{3+} nanofibers with the outer diameter averaging 184 ± 26 nm that gave peaks in the red at 628 and 618 nm under excitation by 260-nm UV light [4]. The optimal Eu^{3+} concentration was 3 mol%. Lu et al. fabricated Y_2O_2S:Yb^{3+}, Er^{3+} nanofibers having the diameter 105 ± 13 nm using polyvinylpyrrolidone. The nanofibers showed strong green and red emission under excitation at 526, 548, and 668 nm, respectively [5].

The Ce^{3+} doped Y_2O_2S:Er^{3+} luminophore can be used to suppress the visible anti-Stokes luminescence when excited in the range 0.90–0.98 μm [6]. The $(Y_{1-x}Er_x)_2O_2S$ solid solutions were found to luminesce in the range 400–2000 nm under excitation with 790- and 810-nm laser beams [7]. The $(Y_{1-x}Eu_x)_2O_2S$ solid solution shows emission in the range 450–1600 nm under 365- nm excitation [8]. In the $Y_{1.80}Er_{0.10}Yb_{0.10}$ O_2S phosphor, visible luminescence was observed when two resonance infrared photons of different energies were absorbed successively [9]. Complex yttrium oxide compounds, whose structures are related to the Y_2O_2S structure, have been studied as optical materials and solid electrolytes [10,11]. The Y_2O_2S:Eu has lower density compared to Gd_2O_2S:Eu [12,13], which allows to consider them as promising biomarkers for living systems. Y_2S_3/ZnO nanocomposites are efficient photocatalysts for decomposition of organic compounds [14]. In an aqueous phase at pH 7, the Y_2S_3 in the composite should partially hydrolyze to yield yttrium oxysulfides. Nanocrystalline Y_2O_3:Eu samples are promising light-emitting-diode materials [15]. Luminescence is also typical of salt compounds of yttrium [16].

The extensive studies of Y_2O_2S-based materials and their practical importance make it topical to investigate the Y_2S_3-Y_2O_3 phase diagram, which will serve as the scientific base of further investigations. Two compounds are formed in the Y_2S_3-Y_2O_3 system: hexagonal Y_2O_2S, space group $P\bar{3}$ml, a = 0.3789 nm, c = 0.6588 nm [17]; and monoclinic Y_2OS_2 ($2Y_2S_3$ $\cdot 1Y_2O_3$), space group $P21/c$, a = 0.8255 nm, b = 0.6885 nm, c = 0.6853 nm, β = 99,63°, z = 4 [18]. "Faint yellow brick-shaped single crystals of Y_2OS_2 were produced as a by-product of oxidizing $YClH_{0.67}$ (or $Na_{0.25}YClH_{0.75}$) by sulfur in a tantalum ampoule at 1123 K for 7 days when oxygen-contaminated starting chlorides (e.g., YOCl) were used [18]."

There have been no intentional studies of Y_2S_3-Y_2O_3 phase diagram

* Corresponding author.

https://doi.org/10.1016/j.jssc.2018.03.001
Received 25 October 2017; Received in revised form 1 March 2018; Accepted 4 March 2018
Available online 10 April 2018

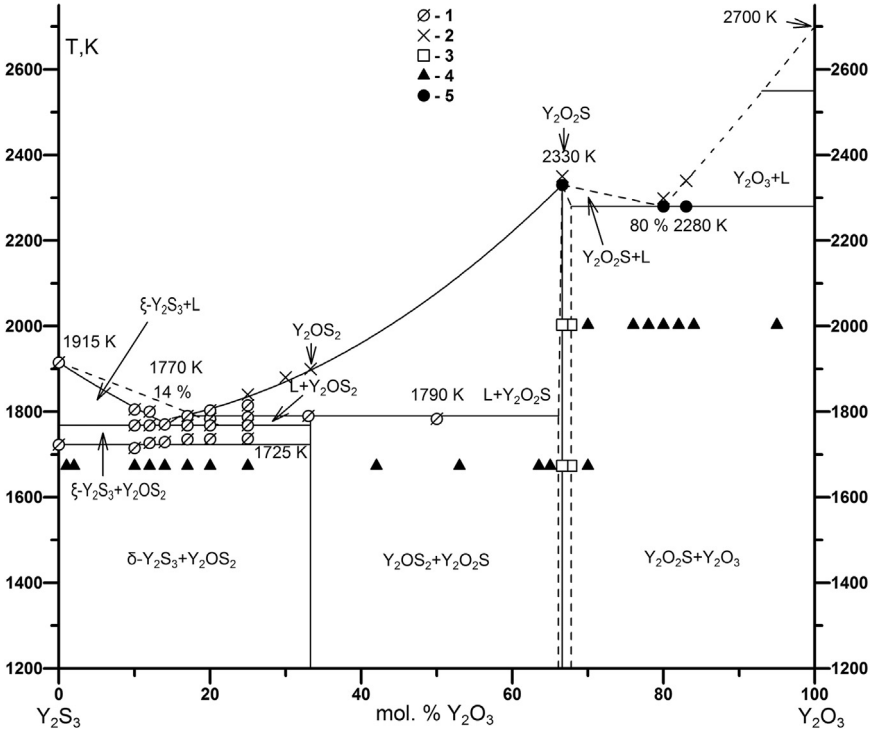

Fig. 1. Phase diagram of the Y_2S_3 - Y_2O_3 system: 1 - complete sample melting; 5 - initiation of sample melting. The state of the samples according to physicochemical data: 2 - single phase: 4 - two phases mixture. DTA/DSC data: 3 - liquidus line temperatures.

as yet. The boundaries of Y_2O_2S-base solid solutions in the Y_2S_3-Y_2O_3 system, the thermal stability of Y_2O_2S and Y_2OS_2, and their melting characters and temperatures were not elucidated. The phase transition enthalpy values can be used to calculate the liquidus lines by the Schroeder equation from the melting temperatures and enthalpies [19].

Sesquisulfide δ-Y_2S_3 crystallizes in monoclinic space group $P2_1/m$ with a = 1.7523 nm, b = 0.4010 nm, c = 1.0173 nm, β = 98.60o, z = 6 [18,20,21] and melts congruently at 2010 K [19,21]. Y_2O_3 has a cubic structure of space group Ia3, a = 1.061 nm, z = 16; it transforms to a hexagonal phase (space group P3m1, a = 0.381 nm, c = 0.609 nm, z = 1) at 2550 K; and melts congruently at 2680 K [22].

Thus, the present study is aimed at the exploration of the phase diagram of Y_2S_3-Y_2O_3 system and determination of enthalpy values for the phase transitions found in the system.

2. Experimental

Monoclinic δ-Y_2S_3 was prepared in the powder by exposing Y_2O_3 (Russia, 99,98 mol% Y_2O_3) to an H_2S + CS_2 flow at 1270–1370 K [23,24]. Gaseous CS_2 and H_2S were prepared by thermal decomposition of NH_4CNS (Russia, 99 mol% NH_4CNS) [25]. The phase transition sequence was observed to be Y_2O_3 → Y_2O_2S → δ-Y_2S_3. The phase constitution of samples was monitored by microstructural analysis (MSA) and X-ray powder diffraction. The presence of even individual Y_2OS_2 crystals in δ-Y_2S_3 was detected by microstructural analysis of sintered or cast samples. We prepared single-phase δ-Y_2S_3 powders with a = 1.7523(8) nm, b = 0.4010(9) nm, c = 1.0173(7) nm, β = 98,60(6)°, which correlates with [18].

Y_2O_2S was prepared in the single-phase powder by consecutively exposing $Y_2(SO_4)_3$ (Russia, 99.98 mol% $Y_2(SO_4)_3$) first to an H_2 flow at 770–870 K for 4 h and then to an H_2S flow at 1170–1220 K for 5 h [26].

The Y_2S_3-Y_2O_3 samples containing 0–60 mol% Y_2O_3 were prepared by alloying Y_2S_3 and Y_2O_2S precursors in graphite crucibles. The 60–100 mol% Y_2O_3 samples were alloyed and annealed in tantalum crucibles. The crucibles were mounted in a silica glass reactor, which was equipped with Al_2O_3 thermal screens. The reactor was pre-evacuated and then filled with Ar (99.998%, Russia) to create an excessive pressure of up to 10 Pa. The thus-prepared cast or sintered samples were then annealed at 1770 K for 0.7–1 h (0–60 mol% Y_2O_3 samples) and for 1 h (60–95 mol% Y_2O_3 samples). When annealed at 1070° C for up to 3000 h, samples were placed in evacuated and sealed-off silica glass ampoules.

Differential scanning calorimetry (DSC) and thermogravimetric analysis (TG) was performed on a STA 449 F3 Jupiter instrument equipped with a W 3%Re - W 25% Re thermocouple in He (99.99999%, Russia) flow (30 ml. per. min.). Sample sizes were 98–103 mg, with the accuracy of an integrated balance equal to ± 0.01 mg. The temperature adjustment accuracy was 0.3 K; the heating rate in the ranges where thermal events were observed was 5 K/min. The results of STA experiments were processed in the Proteus-6 program package. The precision in the phase transition enthalpy determination was ± 18%. In visual polythermal analysis (VPTA), a 40–50 mg sample was placed in a tantalum crucible, which was then mounted on a W 5%Re - W 35% Re thermocouple. VPTA experiments were carried out under argon atmosphere (99.998%); the heating rate was 15–30 K/min. The references used were SrF_2 (T = 1750 K), Pt (T = 2033 K), Cr (T = 2180 K), and Al_2O_3 (T = 2326 K) [27,28].

X-ray powder diffraction patterns were recorded on a DRON-7 using CuKα radiation. Unit cell parameters were calculated in the PDWin-4 program. Microstructures were observed on polished samples using an AxioVert. A1MAT microscope (the AxioVision SE64 program). Microhardness was measured on an HMV-G21DT tester (NaCl reference, H = 791 HV) under the load 490.4 mN. The chemical composition of grains in samples and grain images were determined using a Jeol 6510 LV scanning electron microscope equipped with an energy-dispersive spectrometric unit [29,30].

3. Results and discussion

We are the first to plot the Y_2S_3-Y_2O_3 phase diagram (Fig. 1), to

Table 1
Mass-balance equations of phase transitions for the Y_2S_3-Y_2O_3 system.

Phase transition	Coordinates		Phase-transition equation	ΔH, J/g, KJ/mol
	Composition	T, K		
Polymorphic transition in Y_2S_3	Y_2S_3	1716	$\varepsilon Y_2S_3 \leftrightarrow \xi\ Y_2S_3$	29; 7.9
Y_2S_3 congruent melting	Y_2S_3	1888	$\xi Y_2S_{3(s)} \leftrightarrow Y_2S_{3(l)}$	150; 41.1
Y_2OS_2 incongruent melting	Y_2OS_2 (33.3 mol% Y_2O_3)	1790	$(0.333Y_2O_3; 0.667Y_2S_3)\ Y_2OS_2 \leftrightarrow 0.66\ L\ Y_2S_3\ (0.16Y_2O_3; 0.84Y_2S_3) + 0.34\ Y_2O_2S$ *SS* $(0.66Y_2O_3; 0.34Y_2S_3)$ (2)	190; 52
Eutectic melting	14 mol% Y_2O_3	1770	$0.58\ Y_2S_3 + 0.42\ Y_2OS_2\ (0.333Y_2O_3; 0.667Y_2S_3) \leftrightarrow L\ (0.14\ Y_2O_3; 0.86\ Y_2S_3)$ (4)	215 57

compose the mass-balance equations of phase transitions in the system, and determine their enthalpies (Table 1, Fig. 1).

The δ-Y_2S_3 samples crystallized from melt are in the single phase state; they have monoclinic space group $P2_1/m$, a = 1.7523(8) nm, b = 0.4010(9) nm, c = 1.0170(7) nm, β = 98.60(6)°. Crystallochemical characteristics of δ-Y_2S_3 sample are match to [18]. The microhardness of the δ-Y_2S_3 phase is 411 ± 7 HV. The DSC curve of a δ-Y_2S_3 sample features two peaks whose shapes have linear portions (Fig. 2a, Table 1). After experiencing the thermal event at 1716 ± 7 K (ΔH = 29 ± 6 J/g, ΔH = 7.9 KJ/mol), the sample becomes polycrystalline (Fig. 2a, Table 1). When being cooled, the sample possesses the δ-Y_2S_3 monoclinic structure and retains its geometric shape. The DSC peak observed at 1716 K appears in both quenched and annealed samples and it is fully repeated upon cooling and in heating-cooling cycles. This peak is due to the polymorphic transition of δ-Y_2S_3 to the unquenchable high temperature polymorph ξ-Y_2S_3. δ-Y_2Se_3 experiences a similar polymorphic transition from δ-Y_2Se_3 to ξ-Y_2Se_3 at 1575 K [27].

The melting peak of the Y_2S_3 sample at 1888 ± 7 K (ΔH = 150 ± 28 J/g, ΔH = 41.1 KJ/mol) has a shape typical of phase transitions that appear as invariant equilibria in the phase diagram (Fig. 2a, Table 1). The mass loss of the sample upon DSC is 0.2 mass %; the phase has the composition $Y_2S_{2.99}$. In a sample cooled after DSC, an Y_5S_7 phase (with which Y_2S_3 is in equilibrium in the Y-Y_2S_3 system) is not detected. The δ-Ln_2S_3 compounds have close values of melting temperatures and melting enthalpies: for δ-Ho_2S_3, T = 1970 K and ΔH = 47.7 KJ/mol; for δ-Er_2S_3, T = 1935 K and ΔH = 42.2 KJ/mol [28,29].

No noticeable Y_2S_3-base solid solutions have been found. The 0.5 and 1 mol% Y_2O_3 samples are comprised of two phases. MSA clearly shows $0.58Y_2S_3 + 0.42Y_2OS_2$ eutectic. In pre-eutectic samples, the temperature of the δ-Y_2S_3 to ξ-Y_2S_3 phase transition is 1720 K, which value is commensurate with the polymorphic transition temperature in Y_2S_3 (1716 ± 7 K).

A single-phase Y_2O_2S (a = 0,3781(5) nm, c = 0,6584(4) nm) powder was heat-treated in tantalum and graphite crucibles. An edged ingot was obtained when the powder was melted in a tantalum crucible at 2300–2400 K. This sample comprised two phases. An Y_2O_2S+Ta eutectic was found in the sample in between 30 and 70 μm primary grains of Y_2O_2S (a = 0.3786 nm, c = 0.6591 nm). The faint yellow

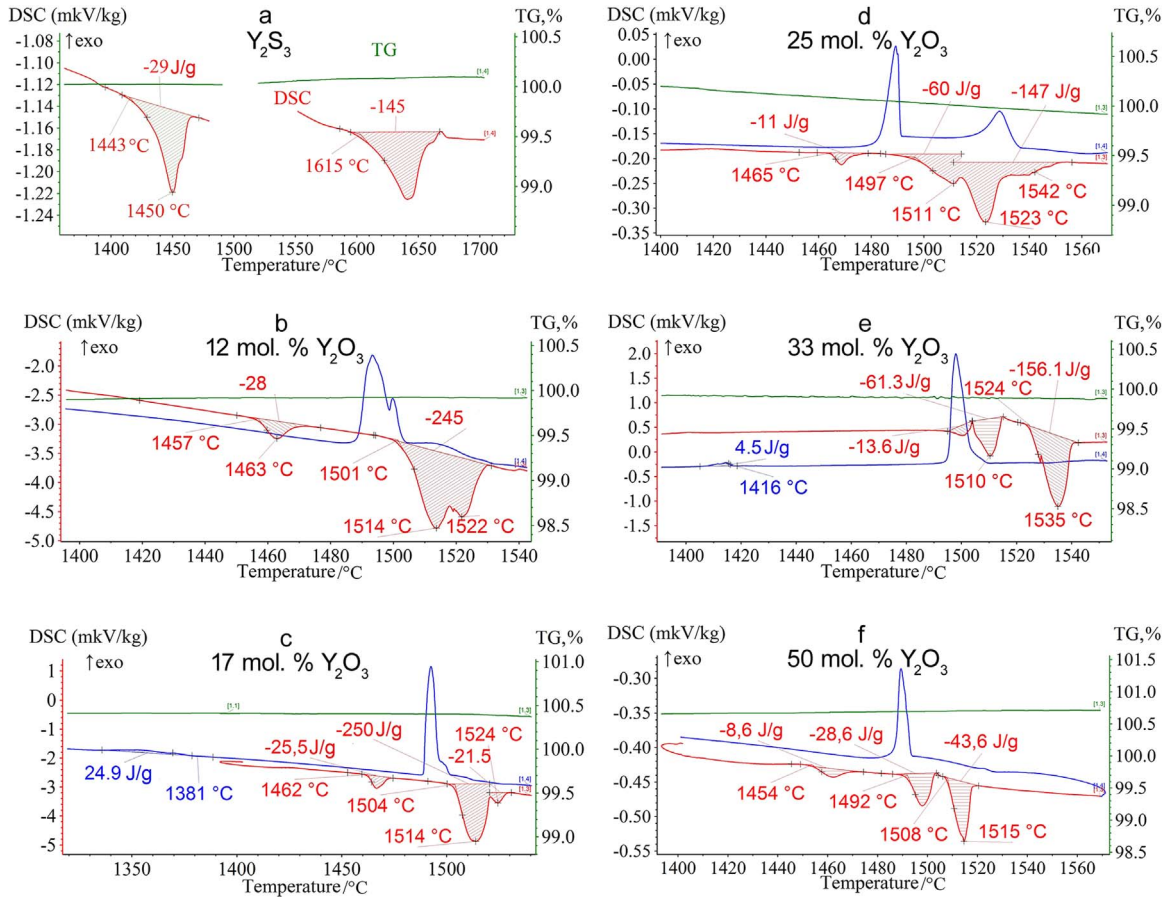

Fig. 2. DSC curves for Y_2S_3 - Y_2O_3 samples. STA 449 F3 Jupiter; heating rate: 5 K/min.

tantalum eutectic grains sized 1–5 μm were flanking Y_2O_2S primary grains.

A compact Y_2O_2S tablet placed inside a graphite crucible can be melted only when the reactor is equipped with a special screen system [30,31]. When the graphite crucible temperature is 2300–2400 K, the cooled sample contains the products of chemical reaction:

$$2Y_2O_2S + C = 2YS + Y_2O_3 + CO\cdot \quad (1)$$

YS grains are golden yellow. Y_2O_3 crystals, transparent in the visible, are dark brawn in the reflected light. YS and Y_2O_3 grains form eutectic mixtures with Y_2O_2S grains, the eutectic being positioned between primary Y_2O_2S grains.

The Y_2O_2S unit cell parameters change noticeably to become a = 0.3804 nm, c = 0.6634 nm. The Ln_2O_2S crystal structure has structural vacancies [32,33]. After reaction (1) occurred, the initially light yellow Y_2O_2S sample becomes dark with a black tinge. The most likely reason behind the increase in Y_2O_2S unit cell parameters is the formation of an introduction solid solution of carbon in the yttrium dioxysulfide structure.

Sintering of Y_2O_2S powders in tantalum crucibles at 1900–2100 K yields single-phase Y_2O_2S samples with a = 0,3784(5) nm, c = 0,6584(4) nm, which are scaled off the walls of crucibles upon shrinkage.

There exists a limited double-sided Y_2O_2S-base solid solution. The 66, 66.7, and 68 mol% Y_2O_3 samples annealed at 1720 K are in single phase state. The average unit cell parameters of Y_2O_2S depend on whether the phase is in equilibrium with Y_2OS_2 or Y_2O_3 phase. The microhardness of Y_2O_2S is 654 ± 7 HV. Y_2O_2S melts congruently at 2350 ± 40 K (VPTA) (Fig. 1).

The Y_2OS_2 ($1Y_2S_3$: $1\ Y_2O_2S$) content in melt-crystallized samples depends on the composition of the sample and the cooling mode. In the Y_2S_3–eutectic (14.5 mol% Y_2O_3) and eutectic-peritectic point on the liquidus curve (16 mol% Y_2O_3) areas, Y_2OS_2 crystallizes directly from melt. The Y_2OS_2 content in the samples of these compositions corresponds to the theoretical yield. In the 14.5 mol Y_2O_3 sample, only Y_2OS_2 and Y_2OS_2 were found by XRD analysis. The contents of chemical elements in grains show that, within one grain, beam falls on Y_2S_3 or Y_2OS_2 phases (Fig. 3). The 17 mol Y_2O_3 sample features primary Y_2O_2S crystals, which do not disappear upon long-term solid-phase anneals (3000 h.).

In the 17–65 mol% Y_2O_3 samples crystallized from melt, the Y_2OS_2 phase is formed by a reaction between Y_2O_2S primary crystals and melt (Table 1 (reaction 2)). Anneals of solidified samples at 1070 K for a period of up to 3000 h does not noticeably (± 5 mol%) increases the Y_2OS_2 content. Samples consist of three phases: Y_2OS_2 and about equal mole fractions of Y_2S_3 and Y_2O_2S (Fig. 4).

The diffraction peaks from the Y_2OS_2 phase were indexed on the basis of data borrowed from [18]: P21/c, a = 0.8256(8) nm, b = 0.6879(8) nm, c = 0.6848(8) nm, β = 99.52(6)°. The calculated unit cell parameters agree with the reported values [18] (Fig. 4). The microhardness of the Y_2OS_2 phase is 491 ± 13 HV. Y_2OS_2 is an incongruently melting compound.

Y_2OS_2 is an incongruently melting compound. The Y_2OS_2 melting peak appears distinctly on DSC curves (Figs. 2d, 2e) at an average temperature of 1790 ± 8 K; ΔH = 190 ± 45 J/g, or ΔH = 52 KJ/mol. A balance equation is composed for Y_2OS_2 incongruent melting (Table 1 (reaction 2)). In the 33–65 mol% samples, there is a nonequilibrium Y_2S_3 phases in the form of eutectic crystals. Melting of the eutectic (0.58 Y_2S_3 + 0.48 Y_2OS_2) (Table 1 (reaction 2)) is manifested on DSC curves as an exotherm. The exotherm can arise only from the reaction of Y_2O_2S crystals with melt (Table 1 (reaction 2)) to yield Y_2OS_2 (Fig. 2d, 2e). The slow cooling rate employed in DSC experiments (5 K/min) creates conditions for Y_2OS_2 to be formed by reaction (2). In a cooled 33 mol% Y_2O_3 sample, there is as much as 50 mol% Y_2OS_2.

The substitution of oxygen for sulfur atoms in yttrium compounds induces a systematic increase in the enthalpy of melting in the series of Y_2S_3 (41.1 KJ/mol) - Y_2OS_2 (52 KJ/mol) - Y_2O_3 (84 KJ/mol) [22].

Y_2S_3 and Y_2OS_2 form an eutectic with composition 14 ± 0.5 mol% Y_2O_3, which corresponds to the phase ratio $0.58Y_2S_3$ + $0.42Y_2OS_2$ (Fig. 4). On polished samples, phase grains have definite colors: Y_2S_3 is light yellowish, and Y_2OS_2 has the same color with a faint grayish tinge. The average melting temperature of the eutectic is 1770 ± 6 K. The enthalpy of melting has a higher than the value calculated by Eq. (2) (Table 1) from the enthalpies of melting of the constituent eutectic phases: ΔH_m = 215 ± 39 J/g against ΔH_m = 167 J/g, respectively.

The liquidus branch from the Y_2S_3 melting point to the eutectic

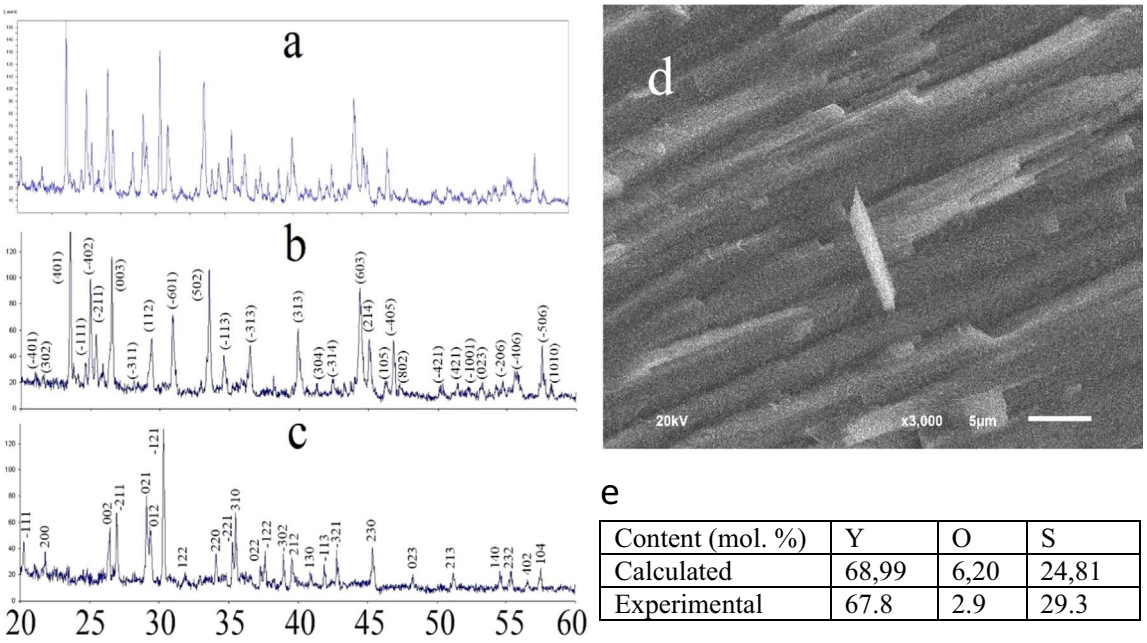

e

Content (mol. %)	Y	O	S
Calculated	68,99	6,20	24,81
Experimental	67.8	2.9	29.3

Fig. 3. (a) X-ray diffraction pattern for a 14.5 mol% Y_2O_3 sample and (b, c) reflections from (b) Y_2S_3 and (c) Y_2OS_2 extracted from this pattern; (d) stands for an average chemical composition of grains of the sample as determined on a Jeol 6510 LV scanning electron microscope.

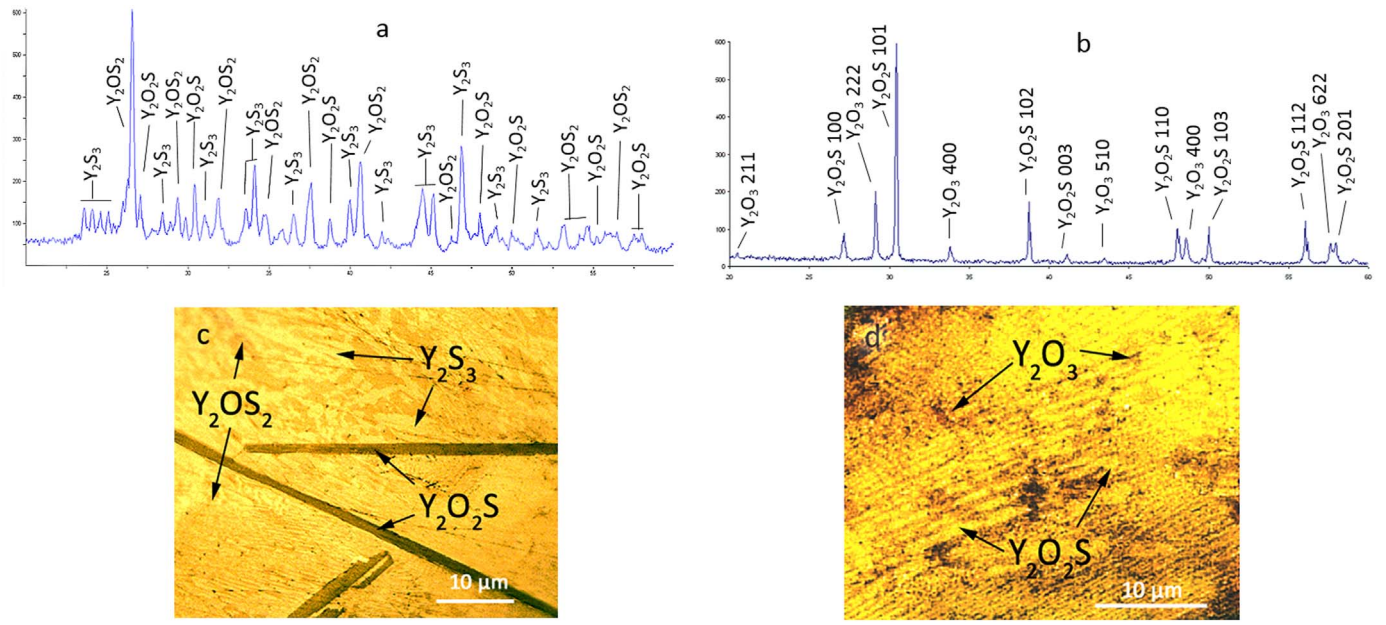

Fig. 4. Chemical and phase () composition of samples that crystallized from melt: a) 18 mol% Y_2O_3 (50 mol% Y_2S_3, 40 mol%, 10 mol% Y_2O_2S); b) 75 mol% Y_2O_3 (71 mol% Y_2O_2S, 29 mol % Y_2O_3). Samples' microstructure: c) 18 mol% Y_2O_3 (there are Y_2O_2S original crystals, eutectic grains of Y_2S_3 (light-colored) and Y_2OS_2 phases); d) 80 mol% Y_2O_3 (there are eutectic grains of Y_2OS_2 (light-colored) и Y_2O_3 phases).

point was drawn using DSC data. The calculation by the Schroeder–Le Chatelier equation (Fig. 1, dashed line) shows its position in case of the eutectic-type Y_2S_3-Y_2O_3 phase diagram [34,35]:

$$\ln x^l = \frac{\Delta H_{melt}}{R}\left(\frac{1}{T_{melt}} - \frac{1}{T}\right) \quad (2)$$

where ΔH_mandT_m are, respectively, the enthalpy of melting and melting temperature of Y_2S_3; and x^l is mole fraction.

The 25 mol% Y_2O_3 sample was melted during a DSC experiment; the liquidus temperature was determined (Fig. 2g). The liquidus line, between the peritectic point and the Y_2O_2S melting point was drawn by DSC and VPTA data. This line has a concave shape.

On TG curves, the mass loss of the 25 mol% Y_2O_3 sample is 0.2 mass % and within 0.1 mass % for the other samples, indicating low thermal volatility of samples (Fig. 2g).

The terminal phases of the Y_2O_2S-Y_2O_3 system form an eutectic. In samples that were melted during heat treatment, the eutectic was built of elongated grains having linear sizes of 1–12 μm (Fig. 4). The eutectic coordinates are 80 ± 1 mol% Y_2O_3, ($0.6Y_2O_2S$ + $0.4Y_2O_3$) and 2150 ± 35 K as determined by VPTA.

The position of yttrium in the lanthanide series next to dysprosium (rY^{3+} (CN 6) = 0.1040 nm; rDy^{3+} (CN 6) = 0.1052 nm [36]) makes it possible to trace the trends of evolution of phase equilibria in the Sm_2S_3 – Sm_2O_3 [37], Gd_2S_3 – Gd_2O_3, and Dy_2S_3 – Dy_2O_3 [38] systems. The Y_2S_3 - Y_2O_3 system possesses a new type of diagram in the Ln_2S_3-Ln_2O_3 series. The compound Y_2OS_2 formed upon crystallization from melt or upon annealing of precursors in the system. Schleid prepared Ln_2OS_2 (Ln = Sm, Gd, Dy, or Y) compounds by reacting the Ln_2OCl precursor with sulfur in a tantalum ampoule at 1070 K for 7 days [18,39]. However, no Ln_2OS_2 (Ln = Sm, Gd, or Dy) were found to form in the reactions of Ln_2S_3 and Ln_2O_2S or upon crystallization from melt, and, respectively, the compounds are not shown in the related phase diagrams. For the yttrium lanthanides (Ln = Gd, Dy, and Y), the extents of Ln_2O_2S-base double-sided solid solutions in Ln_2S_3 – Ln_2O_3 systems are within 2 mol% Ln_2O_3. All Ln_2O_2S compounds melt congruently. The Ln_2O_2S melting temperatures, as determined by VPTA, have similar values: 2320 K for Nd_2O_2S, 2370 K for Sm_2O_2S, 2350 K for Gd_2O_2S, 2350 K for Dy_2O_2S, 2340 K for Er_2O_2S, and 2360 K for Lu_2O_2S.

Thus, in the Ln_2S_3 – Ln_2O_3 systems the thermal stability of Ln_2OS_2 and the evolution trends of the Ln_2S_3 – Ln_2O_3 phase diagrams should be evaluated as a function of rLn^{3+}.

4. Conclusion

The compounds formed in the Y_2S_3-Y_2O_3 system are monoclinic yttrium oxide disulfide Y_2OS_2, which decomposes incongruently at 1790 ± 8 K (ΔH = 190 ± 45 J/g, ΔH = 52 KJ/mol), and hexagonal yttrium dioxide sulfide Y_2O_2S, which melts congruently at 2350 ± 40 K. The following eutectics are formed in the system: 14.0 ± 0.5 mol% Y_2O_3 ($0.58Y_2S_3$ + $0.42Y_2OS_2$), 1770 ± 6 K, ΔH_m = 215 ± 39 J/g, 57 KJ/mol and 80 ± 1 mol% Y_2O_3 ($0.6Y_2O_2S$ + $0.4Y_2O_3$), 2150 ± 40 K. The reactivities of phases have been characterized.

References

[1] Yu.V. Orlovskii, K.K. Pukhov, M.V. Polyachenkova, P.P. Fedorov, O.K. Alimov, E.I. Gorokhova, V.A. Demidenko, O.A. Khristich, R.M. Zakalyukin, T.T. Basiev, J. Lumin. 125 (2007) 201.
[2] A.N. Gruzintseva, C. Barthoub, P. Benalloulb, J. Semicond. 42 (2008) 358.
[3] L. Yang, J. Wang, X. Dong, G. Liu, W. Yu, J. Mater. Sci. 48 (2013) 644.
[4] L. Han, M. Pan, Y. Lv, Y. Gu, X. Wang, D. Li, O. Kong, X. Dong, J. Mater. Sci.: Mater. Electron. 26 (2015) 677.
[5] X. Lu, M. Yang, L. Yang, Q. Ma, X. Dong, J. Tian, J. Mater. Sci.: Mater. Electron. 26 (2015) 4078.
[6] O. Ya Manashirova, A.N. Georgobiani, V.B. Gutana, J. Inorg. Mater. 49 (2013) 278.
[7] O. Ya Manashirova, E.M. Zvereva, A.N. Lobanov, J. Inorg. Mater. 52 (2016) 186.
[8] A.N. Gruzintsev, J. Inorg. Mater. 50 (2014) 885.
[9] A.N. Georgobiani, V.B. Gutan, M.A. Kazaryan, A.V. Krotov, Y.P. Timofeev, O.Y. Manashirov, J. Inorg. Mater. 45 (2009) 1166.
[10] M. Fabián, B. Antić, V. Girman, M. Vučinić-Vasić, A. Kremenović, S. Suzuki, H. Hahn, V. Šepelák, J. Solid State Chem. 230 (2015) 42.
[11] J.A. Lussier, G. Devitt, K.M. Szkop, M. Bieringer, J. Solid State Chem. 242 (2016) 126.
[12] S.A. Osseni, S. Lechevallier, M. Verelst, P. Perriat, J. Dexpert-Ghys, D. Neumeyer, R. Garcia, F. Mayer, K. Djanashvili, J.A. Peters, E. Magdeleine, H. Gros-Dagnac, P. Celsis, R. Mauricot, Nanoscale 6 (2014) 555.
[13] S.A. Osseni, S. Lechevallier, M. Verelst, C. Dujardin, J. Dexpert-Ghys, D. Neumeyer, M. Leclercq, H. Baaziz, D. Cussac, V. Santran, R. Mauricot, J. Mater. Chem. 21 (2011) 18365.
[14] A. Senthilraja, B. Krishnakumar, S.A. Nawabjan, A.J. Sobral, B. Subash, M. Swaminathan, M. Shanthi, J. Water Process Eng. 12 (2016) 32.
[15] C. Waite, R. Mann, A.L. Diaz, J. Solid State Chem. 198 (2013) 357.
[16] F. Yang, Y. Liu, X. Tian, G. Dong, Q. Yu, J. Solid State Chem. 225 (2015) 19.
[17] P.O. Andreev, E.I. Sal'nikova, I.M. Kovenskii, Inorg. Mater. 50 (2014) 1102.

[18] T. Schleid, Eur. J. Solid State Inorg. Chem. 29 (1992) 1015.
[19] N.A. Khritokhin, O.V. Andreev, E.A. Olennikov, T.M. Burkhanova, Rus. J. Inorg. Chem. 47 (2002) 123.
[20] O.V. Andreev, N.N. Parshukov, A.V. Kertman, T.M. Kislovskaya, Rus. J. Inorg. Chem. 41 (1996) 284.
[21] O.V. Andreev, O. Yu Mitroshin, N.A. Khritokhin, I.A. Razumkova, Rus. J. Inorg. Chem. 53 (2008) 440.
[22] M. Fabian, B. Antic, V. Girman, J. Solid State Chem. 230 (2015) 42.
[23] V.G. Bamburov, O.V. Andreev, Rus. J. Inorg. Chem. 47 (2002) 598.
[24] Y. Haibin, J. Zhang, Y.U. Ruijin, S.U. Qiang, J. Rare Earths 27 (2) (2009) 308.
[25] O.V. Andreev, P.V. Miodushevscy, R. Serlenga, N.N. Parsukov, J. Phase Equilibria Diffus. 26 (2005) 109.
[26] P.O. Andreev, E.I. Sal'nikova, O.V. Andreev, Yu.G. Denisenko, I.M. Kovenskii, Inorg. Mater. 53 (2017) 200.
[27] O.V. Andreev, V.B. Kharitontsev, A.A. Polkovnikov, A.V. Elyshev, P.O. Andreev, J. Solid State Chem. 230 (2015) 186.
[28] P.O. Andreev, A.A. Polkovnikov, Yu.G. Denisenko, O.V. Andreev, T.M. Burkhanova, L.A. Pimneva, J. Therm. Anal. Calorim. 131 (2) (2018) 1545.
[29] O.V. Andreev, O. Yu Mitroshin, I.A. Razumkova, Rus. J. Inorg. Chem. 52 (2007) 1161.
[30] O.V. Andreev, V.V. Ivanov, A.V. Gorshkov, P.V. Miodushevskiy, P.O. Andreev, Eurasia. Chem.-Technol. J. 18 (2016) 55.
[31] V.V. Socolov, A.A. Kamarzin, L.N. Trushnikova, M.V. Savelyeva, J. Alloy. Compd. 225 (1995) 567.
[32] G.M. Kuzmicheva, I.V. Perepelkin, A.A. Eliseev, Rus. J. Inorg. Chem. 30 (11) (1985) 2981.
[33] G.M. Kuzmicheva, I.V. Perepelkin, N.V. Porotnikov, D.S. Kholodnyi, Rus. J. Inorg. Chem. 32 (3) (1987) 741.
[34] V.I. Lutsyk, V.P. Vorob'eva, Rus. J. Inorg. Chem. 61 (2016) 188.
[35] N.A. Khritohin, O.V. Andreev, O.V. Mitroshin, A.S. Korotkov, J. Phase Equilibria Diffus. 25 (2004) 515.
[36] R.D. Shannon, Acta Cryst. 32 (1976) 751.
[37] O.V. Andreev, A.S. Vysokikh, V.G. Vaulin, Rus. J. Inorg. Chem. 53 (2008) 1320.
[38] P.O. Andreev, P.P. Fedorov, Rus. J. Inorg. Chem. 58 (2013) 724.
[39] J. Wontcheu, Th. Schleid. Z. Kristallogr. 218 (203). 285.